Geophysical Research Letters

RESEARCH LETTER
10.1029/2018GL081441

Underwater Ice Terrace Observed at the Front of Glaciar Grey, a Freshwater Calving Glacier in Patagonia

Shin Sugiyama[1], **Masahiro Minowa**[2], **and Marius Schaefer**[2]

[1]Institute of Low Temperature Science, Hokkaido University, Sapporo, Japan, [2]Instituto de Ciencias Físicas y Matemáticas, Facultad de Ciencias, Universidad Austral de Chile, Valdivia, Chile

Key Points:
- Subaqueous calving front of a Patagonian glacier was captured by a side-scanning sonar
- Glacier front forms a terrace-like structure in the lake
- Buoyant force acting on the underwater ice promotes large-scale calving

Supporting Information:
- Supporting Information S1

Correspondence to:
S. Sugiyama,
sugishin@lowtem.hokudai.ac.jp

Citation:
Sugiyama, S., Minowa, M., & Schaefer, M. (2019). Underwater ice terrace observed at the front of Glaciar Grey, a freshwater calving glacier in Patagonia. *Geophysical Research Letters*, *46*, 2602–2609. https://doi.org/10.1029/2018GL081441

Received 28 NOV 2018
Accepted 4 FEB 2019
Accepted article online 12 FEB 2019
Published online 6 MAR 2019

Abstract Underwater ice geometry at the front of calving glaciers provides crucial information for calving and underwater melting. In this study, we present ice geometry captured by operating a side-scanning sonar near the front of Glaciar Grey, a freshwater calving glacier in Patagonia. The observations revealed ice projecting into the lake with a substantially different structure from that of known tidewater glaciers. Terrace-like ice structures were found at several tens of meters below the water surface and extended up to 100 m from the aerial ice front. The structure depicted by the sonar was confirmed when the ice front was exposed by flotation during a major calving event. We infer that buoyant force acting on the submerged ice terrace acted as a driver of the calving event. Our study demonstrates the importance of the underwater ice geometry, which affects sizable calving at the front of freshwater calving glaciers.

Plain Language Summary Glaciers terminating in lakes and the ocean are in general retreating more rapidly than glaciers on land. This is because such glaciers lose ice by discharging icebergs and melting in water. The shape of the submerged part of the ice front provides important information for understanding iceberg production and melting, but measurements near the glacier front are difficult to obtain. In this study, we used a side-scanning sonar to visualize underwater ice of a lake terminating glacier in Patagonia. The observations revealed ice jutting into the lake, forming terrace-like structures several tens of meters below the water surface. The structure was significantly different from that of ocean terminating glaciers. The observation was confirmed when the ice front was detached from the glacier and exposed by flotation. Our study demonstrates that buoyant force acting on the ice terrace plays a key role in the production of large icebergs at the front of freshwater calving glaciers.

1. Introduction

Calving glaciers change more rapidly than land-terminating glaciers (e.g., Post et al., 2011) and thus play a central role in global sea level rise (e.g., Burgess et al., 2013; Dussaillant et al., 2018; Howat & Eddy, 2011; Malz et al., 2018; Nuth et al., 2013). Among the calving glaciers, those terminating in freshwater have drawn less attention as compared to tidewater glaciers. Accordingly, little is known about processes at the boundary of the glacier front and freshwater, and the ways in which they differ from a tidewater setting are poorly understood. Freshwater calving glaciers are commonly observed in Patagonia, Alaska, and New Zealand. For instance, more than half of outlet glaciers in the Patagonia Icefield flow into lakes (Aniya, 1988; Aniya et al., 1996; Rignot et al., 2003). Most of these freshwater calving glaciers are receding over the last several decades (e.g., Sakakibara & Sugiyama, 2014; White & Copland, 2015). Some of the glaciers are rapidly retreating and thinning, affecting recent mass loss in Patagonia (e.g., Dussaillant et al., 2018; Malz et al., 2018). Studies in Alaska have shown that some of the freshwater calving glaciers are retreating more rapidly than tidewater glaciers in the region (Larsen et al., 2015). Moreover, occurrence of freshwater calving is increasing in other regions because proglacial lakes are forming after glacier retreat (Carrivick & Tweed, 2013). The study of frontal ablation, that is, calving and underwater melting at the ice-freshwater interface, presents a great challenge for achieving a better understanding of rapidly changing freshwater calving glaciers (Sugiyama et al., 2016).

Underwater ice geometry is the key to understanding the processes occurring at the calving front, since the shape of the ice cliff plays a critical role in the frequency and type of calving (e.g., van der Veen, 2002). It also affects water circulation and subaqueous melting (e.g., Truffer & Motyka, 2016). Nevertheless, only a small amount of observational data is available from a limited number of glaciers because a submerged glacier front is difficult and dangerous to survey. Only recently was a multibeam sonar system operated near the

calving front of tidewater glaciers in Greenland (Fried et al., 2015; Rignot et al., 2015). The measurements showed that the ice front is undercut below the water surface under the influence of rapid subaqueous melting driven by upwelling subglacial meltwater discharge (Motyka et al., 2003, 2013). The observed underwater ice geometry affects calving because the ice overhanging above the undercut is unstable. Observations at freshwater calving glaciers in New Zealand showed significantly different underwater ice geometry. Formation of a subaqueous "ice ramp," that is, an ice front sloping into a water body and extending for several hundred meters to the lake bottom, was reported based on water depth and subbottom profiler surveys (Purdie et al., 2016; Robertson et al., 2012; Warren & Kirkbride, 1998). A similar feature named "ice foot" was reported in Alaska, where a ~20-m-thick and ~50-m-long debris-rich basal ice, projecting into water from the base of a temperate tidewater glacier, was found using a remotely operated vehicle (Hunter & Powell, 1998). They speculated that the ice foot formation was due to its resistance to fracture and/or its stability due to freezing on the sea floor, but it is not clear whether this commonly occurs at other glaciers.

To investigate underwater ice geometry at the front of a freshwater calving glacier, we operated a side-scanning sonar near the front of Glaciar Grey in the Southern Patagonia Icefield. Our data demonstrated that the ice front was projecting into lakewater, forming an up to 100-m-long ice terrace. Based on hydrographic data and observations of a calving event, we discuss the formation mechanism of the ice terrace and its importance in freshwater calving.

2. Study Site

Glaciar Grey (50.9°S, 73.3°W) is situated in the Southern Patagonia Icefield, covering an area of 243 km^2 (De Angelis, 2014; Figure 1a). The glacier flows into a lake named Lago Grey (38.6 km^2 in 2019) through three distinctive termini at present. The focus of this study is the eastern terminus, which is in contact with the eastern arm of the lake along the 850-m-wide calving front (Figures 1b, 1c, and 2a). Ice flow speed is 200–300 m/year at about 1 km from the front (Sakakibara & Sugiyama, 2014; Schwalbe et al., 2017). The eastern terminus has retreated by ~2 km since the 1980s, a retreating trend similar to that of the other two termini and other glaciers in Patagonia (Rivera & Casassa, 2004; Sakakibara & Sugiyama, 2014; Yamamoto, 2018). Based on our water depth sounding, the maximum depth near the glacier is approximately 300 m (Figure 1b).

3. Methods

3.1. Side-Scanning Sonar

We operated a portable side-scanning sonar (0.83 m long and 5.4 kg excluding ballast) (Imagenex Technology Corp. Model 872; Figure S1a) near the front of Glaciar Grey on 31 January 2016 and 11 March 2017. The device was developed for surveying materials and environments at the bottom of water (e.g., Blondel, 2009). The sonar emits a sonic wave beam sideways from a transducer mounted on the tail. In the setting used in this study, wave frequency was 260 Hz, pulse repetition interval was 290 ms (3.4 Hz), the beam center was inclined by 20° from the horizontal, and the beam widths were 2.2° and 75° in the horizontal and vertical planes, respectively (Figure S1b).

We used a motorboat to tow the sonar with its 5-m-long signal cable. The boat was operated at a speed of ~1–2 m/s along the glacier front at a distance usually less than 100 m. Two-way travel time of return signals was converted to the distance to the underwater objects with software provided by the manufacturer, so that a two-dimensional underwater structure was projected on a horizontal plain image (Figure S1b). We used a sound velocity of 1,424 m/s for the conversion, based on the lakewater temperature measured at T1 (Figure 1b; 4.4 °C as a mean in the upper 50 m; Belogol'skii et al., 1999). The maximum range of the sonar echo sounding was 200 m with a resolution of 0.2 m. Acquired data were postprocessed with horizontal coordinates obtained by GPS (Global Positioning System) synchronized with the sonar survey. Software (Chesapeake Technology, SonarWiz) was used to map the sonar signals on to a real space, based on the position and azimuth of the boat given by the GPS. Accuracy of the single-positioning GPS is within several meters in general.

3.2. Water Temperature and Turbidity

Lakewater temperature and turbidity were measured on 9 March 2017 within 250–1,750 m from the glacier front (Figure 1b). We used a temperature, turbidity, and depth profiler (JFE Advantec, ASTD101) to obtain

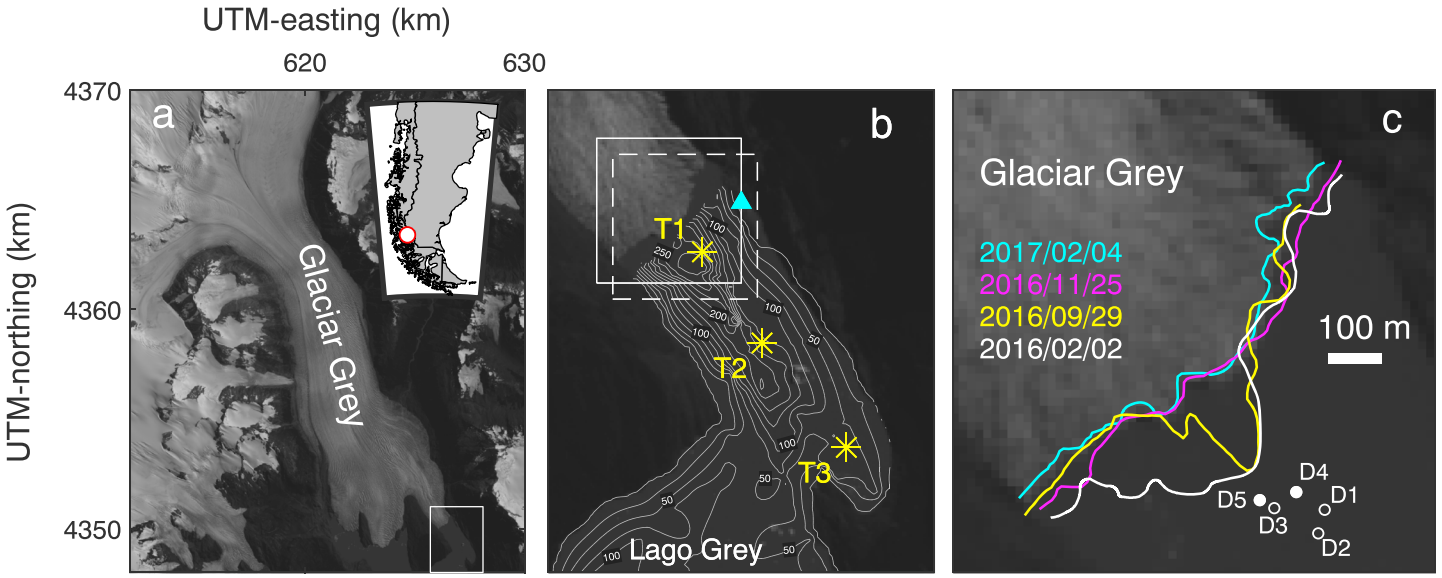

Figure 1. (a) Satellite image (Landsat 8, 4 February 2017) showing Glaciar Grey and its location in South America. The box shows the area covered by (b). Coordinates are in WGS 84/UTM zone 18S. (b) Lakewater temperature and turbidity were measured at (*), and the photographs in Figure 3 were taken at (▲). The boxes indicate the areas shown in Figures 1c and 2d (solid), and in Figure 2c (dashed). Contour lines show the lake bathymetry with intervals of 25 m. (c) Glacier front positions as observed in Landsat 8 satellite images acquired from 2 February 2016 to 4 February 2017. Markers show the locations of water depth profiler measurements. The solid markers indicate that the sites were above underwater ice.

the water properties from the surface to the bottom. The profiler was lowered from the boat to record data every 1 s, which was equivalent to a resolution of 0.2–1 m in depth. The accuracy of the depth, temperature, and turbidity measurements were ±1.8 m, ±0.01 °C, and ±0.3 FTU (formazin turbidity unit) or 2% of measured turbidity, respectively.

3.3. Lakewater Depth

Water depth of Lago Grey was measured in March 2017 over several kilometers from the eastern terminus (Figure 1b). We used an ultrasonic echo sounder (Lowrance HDS-7) operated with an 80- to 130-kHz frequency-modulated transducer (Airmar B75M) mounted on the boat. Depth was recorded by the sounder every 1 s, together with horizontal coordinates obtained from a built-in single-positioning GPS. The accuracy of the depth sounding with a similar device was reported as ~5 m or ~5% of the depth based on measurements in Patagonian lakes (Sugiyama et al., 2016). In addition to the sonar sounding, water depth near the glacier front was measured by lowering the depth profiler to the floor. This measurement was carried out during the side-scan sonar survey on 31 January 2016 at five locations within 200 m of the calving front (Figure 1c).

3.4. Satellite Data

Glacier front positions were retrieved analyzing images acquired by the Landsat 8 Operational Land Imager on 2 February 2016, 29 September 2016, 25 November 2016, and 4 February 2017. Calving front of the eastern terminus was manually delineated, using geographic information software QGIS. The accuracy of the front mapping was equivalent to the image resolution (15 m). The glacier surface elevation near the front was obtained from a DEM (digital elevation model) generated by processing a stereo pair image of ASTER (Advance Spaceborne Thermal Emission and Reflection Radiometer) acquired on 23 October 2016. The resolution of the DEM was 30 m.

4. Results

4.1. Side-Scanning Sonar Image

An intriguing feature captured by the side-scanning sonar was glacier ice below the water surface projecting into the lake. As an example given in Figure S1c, the first echo from the right side of the sonar is a

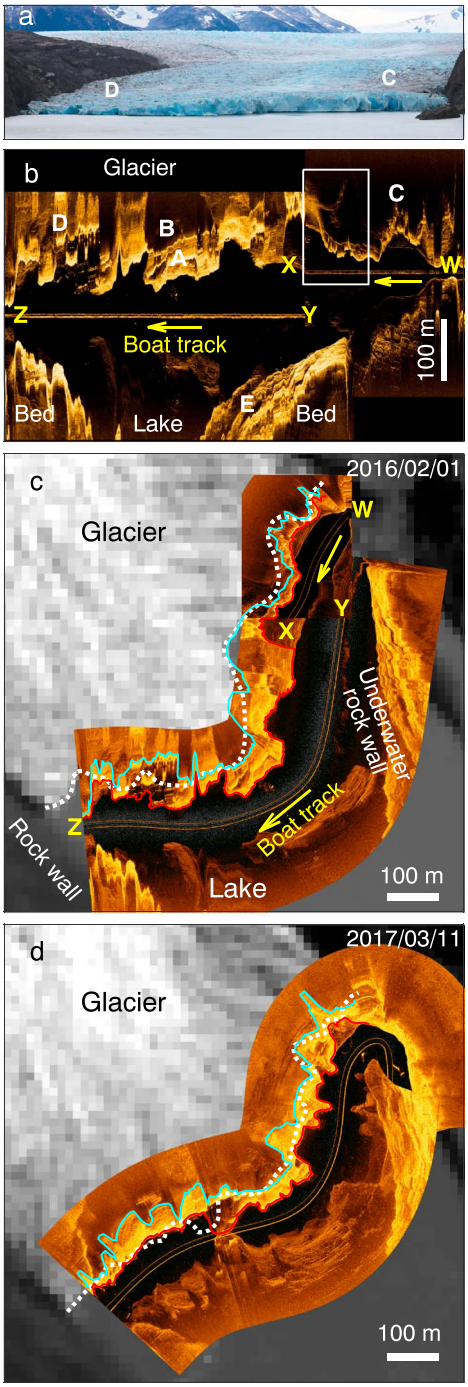

Figure 2. (a) Calving front of Glaciar Grey (1 February 2016). (b) A composite of two side-scanning sonar images acquired on 31 January 2016. Trajectories of the sonar are indicated by lines W-X and Y-Z. The horizontal dimension of the diagram approximately covers the entire glacier front. The box shows the area covered by Figure S1c. (c) The side-scanning sonar image shown in (b) as projected on the UTM coordinate system. Highlighted are ice front positions in water (red), at the water surface (cyan), and as observed by a satellite image (Landsat 8 on 2 February 2016 shown in the background; dotted). W, X, Y, and Z correspond to those in (b). (d) Side-scanning sonar image acquired on 11 March 2017 projected and highlighted as in (c). Landsat 8 image on 4 February 2017 was used for the front position (dotted) and shown in the background.

reflection from the nearest ice surface in the water. The reflection signal extends further from the sonar until the echo weakens at several tens of meters from the first signal. This boundary to the low-reflection zone (dashed line in Figure S1c) is interpreted as being the intersection of the calving front and the water surface. The region between the first signal and the low-reflection zone corresponds to a submerged ice surface. The return signal from this surface is weak, which indicates a relatively large beam incident angle, that is, the underwater ice forms a near-horizontal flat terrace.

Similar ice geometry was observed all along the calving front (Figure 2b). Near the glacier center, the distance from a high/low-reflection boundary (between A and B in Figure 2b) to the outer edge of the ice terrace was approximately 100 m. A similar feature extended along the glacier front toward the northeastern margin (C in Figure 2b), where ice above water was thicker than in the other regions (C in Figure 2a and Figure S2a in the supporting information). The sonar image from the southwestern part showed a number of high-contrast reflectors (D in Figure 2b), suggesting a fractured structure with cracks, trenches, and protrusions. Ice above water was relatively thin in this region (D in Figure 2a), and the calving front was characterized by ice blocks separated by crevasses (Figure S2b) and melt tunnels (Figure S2c). On the other side of the boat track, the sonar image captured an underwater rock wall sloping down from the valley side (E in Figure 2b).

After mapping the sonar image on a real space, the ice front at the water surface and the outer margins of the underwater ice terrace were delineated. The ice front at the water surface approximately matches the glacier front position determined from the satellite image acquired 2 days after the sonar observation (Figure 2c). The subaerial calving front was fringed by underwater ice terraces, and the lengths of the ice reached 100 m at several places. The area of the terrace was 4.9×10^4 m^2 when it was projected on to a horizontal plane (area between the cyan and red lines in Figure 2c). The 30-m mean length of the underwater terrace was obtained by dividing the area by the length along the calving front, or 57 m when the area was divided by the glacier width.

The presence of ice projecting under the water was confirmed by water depths measured near the glacier (Table S1). When it was lowered into the lake, the water profiler hit an ice floor at depths of 25 and 69 m at ~50–100 m from the ice cliff (D4 and D5 in Figure 1c). Depth was 270–301 m at ~30–100 m further offshore (D1–D3 in Figure 1c), which is well in line with the lake depth measurement by the sonar sounding. Further evidence of ice terrace formation was the presence of ice blocks stranding near the calving front (Figure S2d). These ice blocks broke off from the calving front and stayed at the same locations, implying grounding on an underwater ice terrace.

4.2. Calving Event on 31 October 2016

After the side-scanning sonar observation in January 2016, the southwestern section of the ice front retreated, leaving the glacier center protruding into the lake (yellow line in Figures 1c and 3a). A large piece of ice detached from the central part of the glacier on 31 October 2016. The surface area of the detached ice was estimated as 2.1×10^4 m^2 from the satellite images on 29 September and 25 November 2016. This calving event

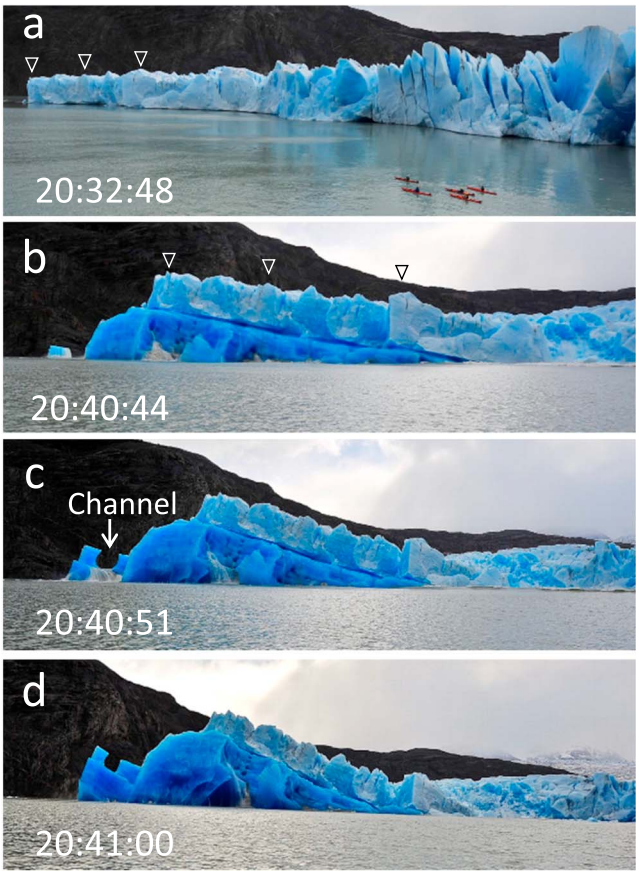

Figure 3. Photographs are of the calving event on 31 October 2016 (taken by Tadeo Sotomayor). Corresponding ice ridges are indicated by the triangles in (a) and (b). Time is in UTC.

was witnessed and photographed by outdoor activity guides from a local tourist company. The photographs provided us with a unique opportunity to observe directly the underwater ice geometry (Figure 3). At 20:40 UTC (17:40 local time) on 31 October, ice broke off at several hundred meters upglacier of the ice front, so that the frontal part of the glacier rotated as a large ice block. The glacier front began moving upward, and underwater ice was lifted and exposed above the water surface (Figure 3b). The photographs show that the ice below the waterline extended from the subaerial ice front by a distance several times longer than the height of the subaerial ice cliff. The ice cliff was 10–20 m high above the lake surface as estimated from the photographs. A circular channel incised on ice was observed deeper in the water (Figures 3c and 3d).

About 4 months after the calving event, we repeated the side-scanning sonar survey on 11 March 2017. The sonar image obtained showed an underwater ice geometry similar the one observed on 31 January 2016, which confirmed the re-formation of an ice terrace within the 131-day period (Figure 2d). The area of the underwater ice terrace was 3.9×10^4 m^2, which was 20% smaller than the first survey. Mean length of the terrace along the frontal margin was 26 m, while that across the glacier width was 46 m.

4.3. Water Property

Our measurements indicated thermal stratification of the lakewater, characterized by a relatively warm near-surface layer situated in the upper ~30 m (Figure 4). Temperature decreases from the surface to the deeper regions and drops below 4 °C at a depth of ~30 m (Figures 4a–4c). Temperature was fairly uniform in the region deeper than 50 m, except for the deepest part at T1. Temperature dropped and turbidity increased below 180 m at T1, showing the accumulation of cold (2.7 °C) and turbid (~100 FTU) water near the lake bottom (Figures 4a and 4d).

5. Discussion

5.1. Underwater Ice Geometry

The side-scanning sonar image indicated that the ice geometry at the front of Grey is substantially different from that reported at tidewater glaciers in Greenland (Fried et al., 2015; Rignot et al., 2015). In contrast to the studies in Greenland, our data showed an up to 100-m-long ice terrace projecting into water (Figure 4d). The vertical dimension of the ice terrace is difficult to measure based on the sonar image. Nevertheless, the water depth near the ice front was 69 and 25 m (Figure 1c and Table S1), indicating that the upper surface of the ice terrace extended several tens of meters below the water surface. The deeper part of the glacier front was beyond the reach of our sonar sounding, but water sharply deepened to ~300 m within only 30–100 m of the ice terrace (Figure 1c and Table S1). Thus, we speculate the ice terrace had a nearly vertical wall in the deeper regions (Figure 4d). The ice geometry exposed by the calving event on 31 October 2016 was consistent with that observed by the side-scan sonar. The photographs taken during the event indicated that the thickness of the ice projecting into water was greater than 50 m (Figures 3b–3d).

Ice front geometry of Glaciar Grey differed in several aspects from ice ramps observed at freshwater calving glaciers in New Zealand. The ice ramps were sloping from the glacier to the lake bed (Dykes et al., 2011; Purdie et al., 2016), whereas at Glaciar Grey the edge of the subaqueous ice terrace dropped sharply toward the lake bottom as confirmed by the depth profiler data. Ice flowed slowly near the front of the glaciers in New Zealand (<30 m/year [Röhl, 2006; Warren & Kirkbride, 2005]) and the front position above water retreated rapidly (from several 10 to >100 m/year [Robertson et al., 2012]). Moreover, subaqueous ice was covered by a thick (5–10 m) debris layer, which insulates the ice from heat for melting

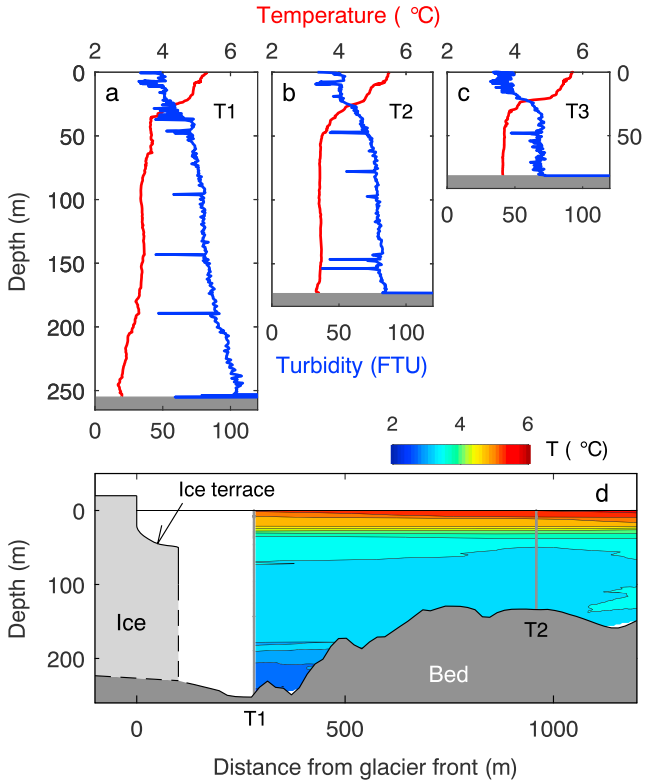

Figure 4. (a–c) Water temperature (red) and turbidity (blue) profiles obtained in Lago Grey at measurement sites (T1–T3) shown in Figure 1b. (d) Water temperature within a vertical cross section along the line connecting the glacier center and the sites T1–T3. Contour intervals are 0.25 °C. The contour map is based on liner interpolation of the profiles obtained at T1–T3.

(Robertson et al., 2012). Thus, ice ramps were considered to consist of stagnant ice remaining after glacier retreat, which had substantially different nature from those observed at the faster flowing Glaciar Grey.

There are very few observations of subaqueous ice geometry available from freshwater calving glaciers in other regions. During the study of large tabular iceberg production at freshwater calving Glaciar Nef in the Northern Patagonia Icefield, Warren et al. (2001) observed subaqueous ice projecting 25 m from icebergs at the depth of 0.2–1.0 m from the water surface. This observation suggests projection of underwater ice at further freshwater calving glaciers in Patagonia and other regions.

5.2. Formation of Underwater Ice Terrace

The stratification of warm water in the upper layer implies enhanced melting near the water surface (Figure 4). Melting below the water surface causes projection of ice above the water. The overhanging ice front which results is unstable and thus facilitates subaerial calving (e.g., Benn et al., 2007). This is a likely mechanism, which maintains the subaerial calving rate of Glaciar Grey, equivalent to the relatively fast speed of ice flow. Lakewater temperature decreased from the surface to the bottom, suggesting a smaller melt rate in the deeper region. The cold and turbid water observed near the lake bottom indicates that cold subglacial discharge stays near the bottom because of higher water density due to sediment load (Figure 4; Sugiyama et al., 2016). In contrast to the front of a tidewater glacier, where upwelling meltwater drives water circulation and draws ocean heat available for subaqueous melting, heat exchange is inactive at the ice-water boundary in a proglacial lake. Thus, we assume that an ice terrace develops because the frontal ablation rate in the deeper region is substantially smaller than the rates in the upper layer and above the water surface.

After the calving event on 31 October 2016, an ice terrace developed to a mean length of 26 m by the time of the second survey on 11 March 2017. The position of the subaerial ice front changed little from November 2016 to February 2017 (Figure 1c), implying that the ice above the water was lost mostly by calving at a rate equivalent to the ice speed (~200–300 m/year), while the ice terrace grew at a rate of >50 m/year. This observation implies a frontal ablation rate of ~150–250 m/year, which is greater than previous estimates for other freshwater calving glaciers in Patagonia (Sugiyama et al., 2016).

5.3. Implication for Calving

Ice extending into water is buoyant and the buoyant force generates a torque and tensile stress in the ice (Warren et al., 2001). The stress causes fracture at the glacier base, resulting in formation and upward propagation of basal crevasses (van der Veen, 1998). Presumably, the calving event on 31 October 2016 was triggered by subglacial and englacial fractures generated by such a process. According to the ASTER-VA DEM on 26 October 2016, the lower 1 km of the glacier tongue sloped gently at ~1.5°. The glacier surface within ~300 m from the calving front was fairly flat and the elevation was approximately 20 m above the lake surface. After the thinning of the glacier, reduction in the overburden load together with the buoyant force acting on the submerged ice terrace facilitated the detachment of a several hundred meters long piece of ice from the glacier. We propose that an underwater ice terrace plays a key role in the frontal ablation of a freshwater calving glacier, by triggering a large-scale calving event, which involves a large volume of underwater ice. Our observations also indicated the importance of subaqueous melting for the frontal ablation. Enhanced melting near the lake surface facilitates large calving by leaving buoyant ice in the water, whereas tidewater calving is enhanced by melt-induced undercutting ice front geometry.

6. Conclusions

Side-scanning sonar survey revealed the shape of the underwater ice at the front of Glaciar Grey, a freshwater calving glacier in Patagonia. Ice extended into water, forming a terrace-like structure at depths of several tens of meters with an extension of up to 100 m from the visible ice front. The observed geometry is substantially different from that of the undercutting ice front recently reported from tidewater glaciers in Greenland. We attribute the differences to the lack of upwelling subglacial discharge and thermal stratification in the proglacial lake. Lakewater temperature was characterized by a near-surface warm layer, which promotes subaqueous melting and facilitates ice terrace formation. The observation of a large calving event confirmed the ice structure as captured by the side-scanning sonar image. The event also demonstrated that buoyant force acting on the submerged ice affects the occurrence of such large-scale calving. Our observations strongly suggest that an underwater ice terrace affects the stability of the terminus. If a glacial lake is also a field of human activity, care should be taken regarding the underwater ice geometry to prevent accident due to sudden emergence of underwater ice by subaqueous calving.

Acknowledgments
The authors express gratitude to T. Sotomayor for providing the photographs taken during the calving event in October 2016. We thank G. Casassa, R. Jana, R. Traub, Y. Yamamoto, and members of the 2016 and 2017 campaigns at Glaciar Grey. Logistic support was offered by Antares Bigfoot Patagonia SA. K. Inose helped the sonar image processing and D. Sakakaibara provided the ice speed data. English text was corrected by Susan Braun-Clarke. We thank two anonymous reviewers for providing constructive comments and the Scientific Editor J. Stroeve for handing the paper. This research was funded by JSPS KAKENHI grant 26550001 (2014–2017), 16H05734 (2016–2020), and 17H06320 (2017–2022). The Landsat 8 images and the ASTER-VA DEM were obtained at http://landsat.usgs.gov/ and https://gbank.gsj.jp/madas. The sonar and water profiler data presented in the paper are available at https://data.mendeley.com/datasets/jpz52pm9sc/1.

References

Aniya, M. (1988). Glacier inventory for the Northern Patagonia Icefield, Chile, and variations 1944/45 to 1985/86. *Arctic and Alpine Research*, *20*(2), 179–187. https://doi.org/10.2307/1551496

Aniya, M., Sato, H., Naruse, R., Skvarca, P., & Casassa, G. (1996). The use of satellite and airborne imagery to inventory outlet glaciers of the Southern Patagonia Icefield, South America. *Photogrammetric Engineering and Remote Sensing*, *62*(12), 1361–1369.

Belogol'skii, V. A., Sekoyan, S. S., Samorukova, L. M., Stefanov, S. R., & Levtsov, V. I. (1999). Pressure dependence of the sound velocity in distilled water. *Measurement Techniques*, *42*(4), 406–413. https://doi.org/10.1007/BF02504405

Benn, D., Warren, C., & Mottram, R. (2007). Calving processes and the dynamics of calving glaciers. *Earth-Science Reviews*, *82*(3-4), 143–179. https://doi.org/10.1016/j.earscirev.2007.02.002

Blondel, P. (2009). *The handbook of sidescan sonar*. Berlin, Heidelberg, and New York: Springer. https://doi.org/10.1007/978-3-540-49886-5

Burgess, E. W., Forster, R. R., & Larsen, C. F. (2013). Flow velocities of Alaskan glaciers. *Nature Communications*, *4*(1), 2146. https://doi.org/10.1038/ncomms3146

Carrivick, J. L., & Tweed, F. S. (2013). Proglacial lakes: Character, behaviour and geological importance. *Quaternary Science Reviews*, *78*, 34–52. https://doi.org/10.1016/j.quascirev.2013.07.028

De Angelis, H. (2014). Hypsometry and sensitivity of the mass balance to changes in equilibrium-line altitude: The case of the Southern Patagonia Icefield. *Journal of Glaciology*, *60*(219), 14–28. https://doi.org/10.3189/2014JoG13J127

Dussaillant, I., Berthier, E., & Brun, F. (2018). Geodetic mass balance of the Northern Patagonian Icefield from 2000 to 2012 using two independent methods. *Frontiers in Earth Science*, *6*, 8. https://doi.org/10.3389/feart.2018.00008

Dykes, R., Brook, M., Robertson, C., & Fuller, I. (2011). Twenty-first century calving retreat of Tasman Glacier, Southern Alps, New Zealand. *Arctic, Antarctic, and Alpine Research*, *43*(1), 1–10. https://doi.org/10.1657/1938-4246-43.1.1

Fried, M. J., Catania, G. A., Bartholomaus, T. C., Duncan, D., Davis, M., Stearns, L. A., et al. (2015). Distributed subglacial discharge drives significant submarine melt at a Greenland tidewater glacier. *Geophysical Research Letters*, *42*, 9328–9336. https://doi.org/10.1002/2015GL065806

Howat, I. M., & Eddy, A. (2011). Multi-decadal retreat of Greenland's marine-terminating glaciers. *Journal of Glaciology*, *57*(203), 389–396. https://doi.org/10.3189/002214311796905631

Hunter, L. E., & Powell, R. D. (1998). Ice foot development at temperate tidewater margins in Alaska. *Geophysical Research Letters*, *25*(11), 1923–1926. https://doi.org/10.1029/98GL01403

Larsen, C. F., Burgess, E., Arendt, A. A., O'Neel, S., Johnson, A. J., & Kienholz, C. (2015). Surface melt dominates Alaska glacier mass balance. *Geophysical Research Letters*, *42*, 5902–5908. https://doi.org/10.1002/2015GL064349

Malz, P., Meier, W., Casassa, G., Jaña, R., Skvarca, P., & Braun, M. H. (2018). Elevation and mass changes of the Southern Patagonia Icefield derived from TanDEM-X and SRTM data. *Remote Sensing*, *10*(2), 188. https://doi.org/10.3390/rs10020188

Motyka, R. J., Dryer, W. P., Amundson, J., Truffer, M., & Fahnestock, M. (2013). Rapid submarine melting driven by subglacial discharge, LeConte Glacier, Alaska. *Geophysical Research Letters*, *40*, 5153–5158. https://doi.org/10.1002/grl.51011

Motyka, R. J., Hunter, L., Echelmeyer, K. A., & Connor, C. (2003). Submarine melting at the terminus of a temperate tidewater glacier, LeConte Glacier, Alaska, U.S.A. *Annals of Glaciology*, *36*, 57–65. https://doi.org/10.3189/172756403781816374

Nuth, C., Kohler, J., König, M., von Deschwanden, A., Hagen, J., Kääb, A., et al. (2013). Decadal changes from a multi-temporal glacier inventory of Svalbard. *The Cryosphere*, *7*(5), 1603–1621. https://doi.org/10.5194/tc-7-1603-2013

Post, A., O'Neel, S., Motyka, R. J., & Streveler, G. (2011). A complex relationship between calving glaciers and climate. *Eos, Transactions American Geophysical Union*, *92*(37), 305–306. https://doi.org/10.1029/2011EO370001

Purdie, H., Bealing, P., Tidey, E., Gomez, C., & Harrison, J. (2016). Bathymetric evolution of Tasman Glacier terminal lake, New Zealand, as determined by remote surveying techniques. *Global and Planetary Change*, *147*, 1–11. https://doi.org/10.1016/j.gloplacha.2016.10.010

Rignot, E., Fenty, I., Xu, Y., Cai, C., & Kemp, C. (2015). Undercutting of marine-terminating glaciers in West Greenland. *Geophysical Research Letters*, *42*, 5909–5917. https://doi.org/10.1002/2015GL064236

Rignot, E., Rivera, A., & Casassa, G. (2003). Contribution of the Patagonia Icefields of South America to sea level rise. *Science*, *302*(5644), 434–437. https://doi.org/10.1126/science.1087393

Rivera, A., & Casassa, G. (2004). Ice elevation, areal, and frontal changes of glaciers from National Park Torres del Paine, Southern Patagonia Icefield. *Arctic and Alpine Research*, *36*(4), 379–389. https://doi.org/10.1657/1523-0430(2004)036[0379:IEAAFC]2.0.CO;2

Robertson, C. M., Benn, D. I., Brook, M. S., Fullier, I. C., & Holt, K. A. (2012). Subaqueous calving margin morphology at Mueller, Hooker and Tasman glaciers in Aoraki/Mount Cook National Park, New Zealand. *Journal of Glaciology*, *58*(212), 1037–1046. https://doi.org/10.3189/2012JoG12J048

Röhl, K. (2006). Thermo-erosional notch development at fresh-water-calving Tasman Glacier, New Zealand. *Journal of Glaciology*, *52*(177), 203–213. https://doi.org/10.3189/172756506781828773

Sakakibara, D., & Sugiyama, S. (2014). Ice-front variations and speed changes of calving glaciers in the Southern Patagonia Icefield from 1984 to 2011. *Journal of Geophysical Research: Earth Surface*, *119*, 2541–2554. https://doi.org/10.1002/2014JF003148

Schwalbe, E., Kröhnert, M., Koschitzki, R., Johnson, E., Cárdenas, C., & Maas, H-G. (2017). Determination of spatio-temporal velocity fields at Grey Glacier using terrestrial image sequences and optical satellite imagery, First IEEE International Symposium of Geoscience and Remote Sensing (GRSS-CHILE), Valdivia, 1–6.

Sugiyama, S., Minowa, M., Sakakibara, D., Skvarca, P., Sawagaki, T., Ohashi, Y., et al. (2016). Thermal structure of proglacial lakes in Patagonia. *Journal of Geophysical Research: Earth Surface*, *121*, 2270–2286. https://doi.org/10.1002/2016JF004084

Truffer, M., & Motyka, R. J. (2016). Where glaciers meet water: Subaqueous melt and its relevance to glaciers in various settings. *Reviews of Geophysics*, *54*, 220–239. https://doi.org/10.1002/2015RG000494

van der Veen, C. J. (1998). Fracture mechanics approach to penetration of bottom crevasses on glaciers. *Cold Regions Science and Technology*, *27*(3), 213–223. https://doi.org/10.1016/S0165-232X(98)00006-8

van der Veen, C. J. (2002). Calving glaciers. *Progress in Physical Geography*, *26*(1), 96–122. https://doi.org/10.1191/0309133302pp327ra

Warren, C., Benn, D., Winchester, V., & Harrison, S. (2001). Buoyancy-driven lacustrine calving, Glacier Nef, Chilean Patagonia. *Journal of Glaciology*, *47*(156), 135–146. https://doi.org/10.3189/172756501781832403

Warren, C., & Kirkbride, M. (1998). Temperature and bathymetry of ice-contact lakes in Mount Cook National Park, New Zealand. *New Zealand Journal of Geology and Geophysics*, *41*(2), 133–143. https://doi.org/10.1080/00288306.1998.9514797

Warren, C., & Kirkbride, M. (2005). Calving speed and climatic sensitivity of New Zealand lake-calving glaciers. *Annals of Glaciology*, *36*, 173–178.

White, A., & Copland, L. (2015). Decadal-scale variations in glacier area changes across the Southern Patagonian Icefield since the 1970s. *Arctic, Antarctic, and Alpine Research*, *47*(1), 147–167. https://doi.org/10.1657/AAAR0013-102

Yamamoto, Y. (2018). Recent frontal variations and driving mechanisms of Glaciar Grey in the Southern Patagonia Icefield, Master thesis, Hokkaido University, Sapporo.